

Received 30 January 2023, accepted 7 March 2023, date of publication 9 March 2023, date of current version 16 March 2023.

Digital Object Identifier 10.1109/ACCESS.2023.3255099

RESEARCH ARTICLE

Detecting Facial Landmarks on 3D Models Based on Geometric Properties—A Review of Algorithms, Enhancements, Additions and Open-Source Implementations

OGUZHAN TOPSAKAL¹, (Member, IEEE), TAHIR CETIN AKINCI^{2,3}, (Senior Member, IEEE), JOSHUA MURPHY¹, TAYLOR LEE-JAMES PRESTON¹, AND MEHMET MAZHAR CELIKOYAR⁴

¹Department of Computer Science, Florida Polytechnic University, Lakeland, FL 33805, USA

²Department of Electrical Engineering, Istanbul Technical University, 34467 Istanbul, Turkey

³Winston Chung Global Energy Center (WCGEC), University of California at Riverside, Riverside, CA 92521, USA

⁴School of Medicine, Department of Otolaryngology, Demiroglu Bilim University, 34394 Istanbul, Turkey

Corresponding author: Tahir Cetin Akinci (tahircetin.akinci@ucr.edu)

This work was supported by the Health Systems Engineering (HSE) Innovative Grant from Florida Polytechnic University (2022).


ABSTRACT Facial landmark detection, a crucial aspect of face recognition, is widely used in various fields, such as facial surgeries, biometrics, and surveillance systems. With the advancement of affordable and capable 3D scanning technologies, research on automatically detecting facial landmarks on 3D models is gaining momentum. Utilizing the geometric properties of 3D facial models, researchers have developed algorithms for various landmarks with varying levels of accuracy. In this study, we reviewed existing literature and developed algorithms for thirty-eight landmarks using geometric properties and statistical information about facial measurements. The algorithms for thirty landmarks are original contributions to the literature. We provide the implementation of all the algorithms as open-source Python code, along with the pseudocode for both our algorithms and those found in the literature. To the best of our knowledge, this study covers the largest number of facial landmark detection algorithms based on the geometric properties of 3D models. This is the first study that provides the implementation of the algorithms along with detailed pseudocode. The results of the algorithms are presented by calculating the mean, median, standard deviation, minimum, and maximum of the errors and depicting the histogram for each landmark over a hundred 3D facial scans. The results show that geometric properties and statistics can be utilized to achieve more robust solutions for facial landmark detection.

INDEX TERMS 3D, landmarks detection, face analysis, geometric, open source, review.

I. INTRODUCTION

The automatic detection of facial landmarks is a crucial aspect of face recognition research, widely used in various fields, including facial surgeries, biometrics, information security, access control for law enforcement, surveillance systems, and smart cards [1].

Current solutions for facial landmark detection mostly work on 2D images (photos). However, as 3D images (scans)

The associate editor coordinating the review of this manuscript and approving it for publication was Khoa Luu .

become more prevalent due to recent advances in technologies and affordability, research on automatically detecting facial landmarks on 3D images is gaining interest among researchers [2]. Using 3D images for facial landmark detection has the potential to overcome challenges faced when using 2D images, such as variations in lighting, posture, expression, and occlusion [3], [4], [5]. The techniques used in the field of facial landmark detection on 3D images have been categorized in various ways by researchers [3], [5], [6], [7]. One recent categorization divides the techniques into two main categories: conventional and deep learning methods.

Conventional techniques can be further divided into three subcategories: local feature-based, holistic-based, and hybrid. Local-based approaches focus on specific facial features, such as the nose and eyes, while holistic-based approaches use the entire face to generate feature vectors for landmark detection. Hybrid methods combine both local and global facial features. For conventional methods, the key step is finding robust feature points and descriptors based on the geometric information of 3D face data [3]. Conventional methods for facial landmark detection also utilize statistical feature models in addition to geometric information [5], [6], [7], [8]. The related work that focuses on geometric information employs four types of methods: curvature analysis, combining 2D texture with 3D shape, matching 3D face templates with a manually marked model to establish correspondences, and using generic image descriptors [5].

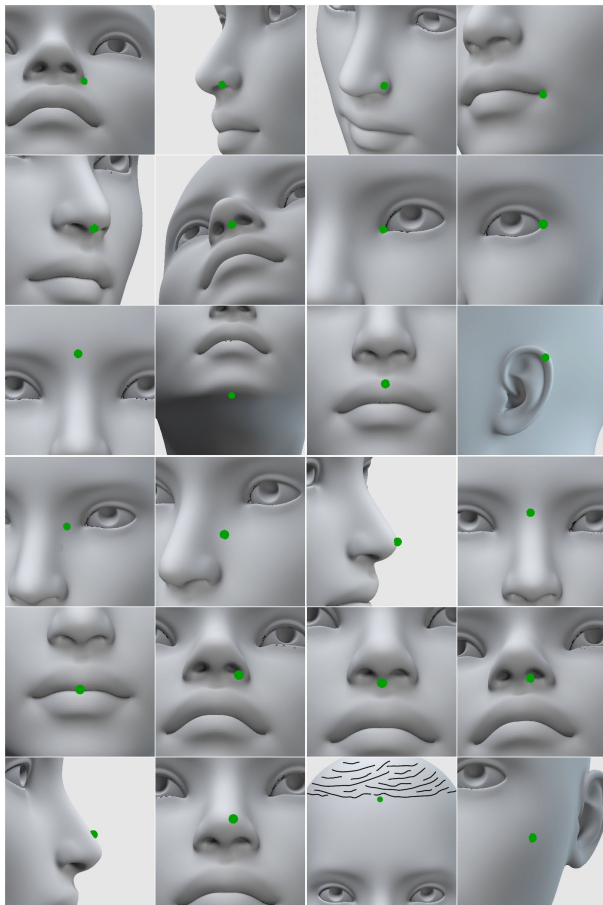


FIGURE 1. The facial landmarks that we studied. The bilateral landmarks are shown only once. From top left to bottom right: Alar Base Junction/Alar Crease, Alar Rim's Highest Point, Alare/Alar Flare, Cheilion, Columellar Break Point, Columellar Rim, Endocanthion, Exocanthion, Glabella, Gnathion, Labiale Superius, Lateral helix of ear, Maxillofrontale, Nasal Parenthesis, Pronasale, Sellion, Stomion, Subalare, Subnasale, Subnasale, Supratip Break Point, Tip Defining Point, Trichion, Zygon.

On the other hand, deep learning methods have been used to provide solutions to find facial landmark locations on 3D images. A common approach to facial landmark detection on 3D scans is to use a 3D CNN (Convolutional Neural Network) which consists of 3D convolutional kernels and 3D pooling

layers [9], [10]. Another approach is to use a combination of a 2D CNN and a 3D morphable model (3DMM) [11], [12], [13], [14]. This method uses the 2D CNN to predict 2D landmark locations on an image of the face, which is then used to fit a 3DMM and estimate the 3D landmark positions.

Machine Learning (and hence deep learning) is recommended to solve complex problems for which using a traditional approach yields no good solution [15]. We believe geometric properties of the face embedded in the 3D face scans can be utilized to accurately locate some of the facial landmarks. Several studies have demonstrated the effectiveness of utilizing geometric and statistical features in facial landmark detection. For instance, Abu et al. [16], Gupta et al. [17], Vezzetti et al. [6], Liang et al. [18], Li et al. [19], and Manal et al. [5] have successfully detected 8, 10, 13, 17, 25, and 30 landmarks, respectively. In this study, we build upon the existing work utilizing the geometric properties of facial features on 3D models [5], [6], [16], [17], [19].

We reviewed the literature and developed algorithms for thirty-eight landmarks utilizing geometric properties and statistical information about facial measurements. Eight of our algorithms were based on existing work, while thirty were original contributions. The implementation of these algorithms is provided as open-source Python code, along with the pseudocode for both our algorithms and those found in the literature. To the best of our knowledge, this study covers the most extensive number of facial landmark detection algorithms based on the geometric properties of 3D models. The accuracy of the algorithms was evaluated using over a hundred 3D facial scans.

II. METHODS AND MATERIALS

Facial features (landmarks) and measurements that are in use by researchers and facial plastic surgeons were presented in a recent literature review article [20] and a free web-based facial analysis tool [21]. While there are over a hundred facial landmarks, we focused on the ones that are more relevant to facial plastic surgery. We consulted with surgeons and asked which measures (distances, angles, and ratios) are most important for facial plastic surgeries, specifically rhinoplasty. Based on their answers, we identified landmarks and also added landmarks that are used for computing visualization about facial symmetry such as endocanthion and exocanthion. Fourteen of the landmarks are bilateral, meaning that they exist on both the left and right sides of the face symmetrically. The total number of facial landmarks adds up to thirty-eight. Figure 1 shows the facial landmarks that we study. The bilateral landmarks are only shown once. While we focus on the landmarks that are mostly around the nose region, most of it is relevant to research on facial surgeries and facial recognition in general.

We reviewed the literature [6], [8], [9], [10], [11], [12], [13], [14], [15], [16], [17], [18], [19], [20], [21], [22], [23], [24], [25], [26], [27], [28], [29], [30], [31], [32], [33], [34], [35], [36], [37], [38], [39], [40] to identify the facial

TABLE 1. Landmarks that have Pseudocode in the literature and if our algorithm is influenced by any or not. The rest of the landmarks that are not listed on this table do not have Pseudocode in the literature and are original.

Facial landmark	Articles that have pseudocode for the landmark	Influenced by or original
Alare/Alar Flare - left/right	[Abu, Ngo, et. al. 2019][16], [Vezzetti, Marcolin 2014] [33], [Liang, Wu, et. al. 2013] [19], [Guo, Mei et. al. 2013] [30], [Berretti, Ben Amor, et. al. 2011] [26], [Gupta, Markey, et. al. 2010] [17], [Vezzetti, E., Marcolin, F., Tornincasa, S. et al. 2018] [18], [M. P. Pamplona Segundo, L. Silva, O. R. P. Bellon and C. C. Queirolo] [25].	Influenced by Liang, Wu, et. al. 2013 and Abu, Ngo, et. al. 2019
Cheilion - left/right	[Liang, Wu, et. al. 2013] [19], [Galvánek, Furmanová, et. al. 2015] [37] [Berretti, Ben Amor, et. al. 2011] [26], [Gupta, Markey, et. al. 2010] [17], [Vezzetti, E., Marcolin, F. 2014] [33].	Original
Endocanthion - left/right	[Vezzetti, Marcolin 2014] [33], [Liang, Wu, et. al. 2013] [19], [Berretti, Ben Amor, et. al. 2011] [26], [Galvánek, Furmanová, et. al. 2015] [37] [Gupta, Markey, et. al. 2010] [17], [Moos, Marcolin, et. al. 2017] [34], [Vezzetti, E., Marcolin, F., Tornincasa, S. et al. 2018] [18], [M. P. Pamplona Segundo, L. Silva, O. R. P. Bellon and C. C. Queirolo] [25].	Original
Exocanthion - left/right	[Vezzetti, Marcolin 2014] [33], [Liang, Wu, et. al. 2013] [19], [Berretti, Ben Amor, et. al. 2011] [26], [Galvánek, Furmanová, et. al. 2015] [37] [Gupta, Markey, et. al. 2010] [17] [Vezzetti, E., Marcolin, F., Tornincasa, S. et al. 2018] [18], [M. P. Pamplona Segundo, L. Silva, O. R. P. Bellon and C. C. Queirolo] [25].	Original
Gnathion	[Manal, Arsalane, et. al. 2019] [5]	Original
Labiale Superius	[Abu, Ngo, et. al. 2019] [16], [Manal, Arsalane, et. al. 2019] [7], [Vezzetti, E., Marcolin, F. 2014] [33].	Influenced by Abu, Ngo, et. al. 2019
Pronasale/Tip	[Abu, Ngo, et. al. 2019] [16], [Vezzetti, Marcolin 2014] [33].	influenced by Abu, Ngo, et. al. 2019
Sellion	[Liang, Wu, et. al. 2013] [19].	influenced by Liang, Wu, et. al. 2013
Stomion	[Abu, Ngo, et. al. 2019] [16], [Manal, Arsalane, et. al. 2019] [7], [Galvánek, Furmanová, et. al. 2015] [37].	influenced by Abu, Ngo, et. al. 2019
Subnasale	[Abu, Ngo, et. al. 2019] [16], [Vezzetti, Marcolin 2014] [33], [Liang, Wu, et. al. 2013] [19], [Guo, Mei et. al. 2013] [30], [Moos, Marcolin, et. al. 2017] [34], [Vezzetti, E., Marcolin, F., Tornincasa, S. et al. 2018] [18].	Influenced by Guo, Mei et. al. 2013

TABLE 2. Facial landmark, their dependent landmarks in the algorithm and the source of statistics used in their Pseudocode.

Facial Landmark	Dependent Landmarks	Source of Statistics
Alar Base Junction/Alar Crease - left/right	Alar flare, Subnasale	Facebase
Alar Rim’s Highest Point - left/right	Subnasale	Proprietary dataset
Alare/Alar Flare - left/right	Pronasale, Subnasale	Facebase
Cheilion - left/right	Stomion, Alar flare	Facebase
Columellar Break Point	Pronasale	Proprietary dataset
Columellar Rim - left/right	Pronasale	Proprietary dataset
Endocanthion - left/right	Sellion	Facebase
Exocanthion - left/right	Sellion	Facebase
Glabella	Pronasale	Facebase
Labiale Superius	Subnasale	Facebase
Lateral helix of ear - left/right	N/A	Facebase
Maxillofrontale - left/right	Pronasale, Endocanthion	Proprietary dataset
Menton/Gnathion	Pronasale	Facebase
Nasal Parenthesis - left/right	Pronasale	Proprietary dataset
Nasion/Radix	Pronasale	Facebase
Pronasale/Tip	N/A	N/A
Sellion	Pronasale	Facebase
Stomion	Labiale Superius	Facebase
Subalare - left/right	Subnasale	Facebase, Proprietary dataset
Subnasale - left/right	Subnasale	Proprietary dataset
Subnasale	Pronasale	Facebase
Supratip Break Point	Pronasale	Proprietary dataset
Tip Defining Point - left/right	Pronasale	Proprietary dataset
Trichion	Glabella	Proprietary dataset
Zygion - left/right	Pronasale	Facebase, Proprietary dataset

landmark detection algorithms on 3D models based on geometric properties.

Pronasale/Tip (prn) was a landmark that was studied the most, followed by other commonly studied landmarks such as Exocanthion, Cheilion, Endocanthion, Nasion/Radix, Subnasale, Labiale Inferius, Labiale Superius. However,

we could not find any pseudocode listed in the literature for the following facial landmarks, and we devised original algorithms for those:

- Alar Base Junction/Alar Crease - left/right
- Alar Rim’s Highest Point - left/right
- Columellar Break Point

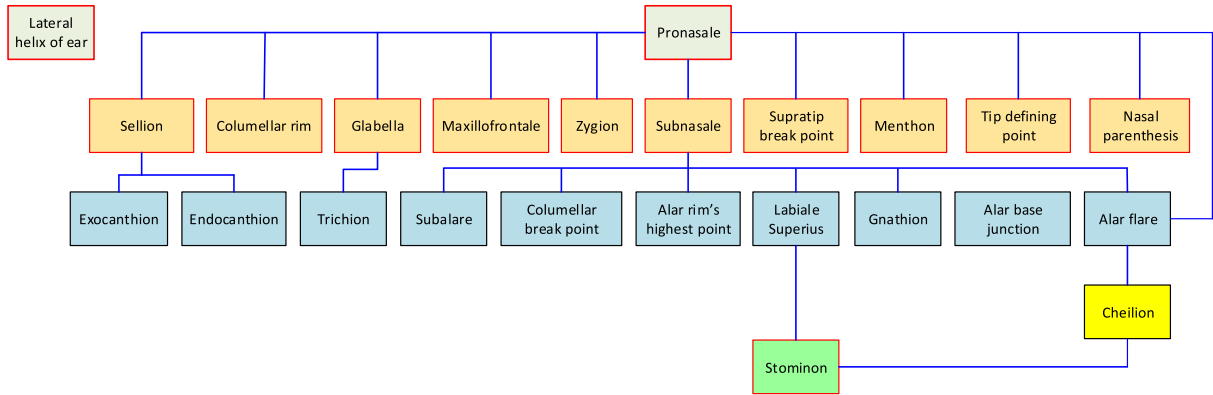


FIGURE 2. The hierarchy of dependencies between the facial landmark algorithms. Lower levels require running the algorithm of the upper levels first.

- Columellar Rim - left/right
- Lateral helix of ear - left/right
- Maxillofrontale - left/right
- Glabella/Menton
- Nasal Parenthesis - left/right
- Nasion/Radix
- Supratip Break Point
- Tip Defining Point - left/right
- Trichion
- Zygion - left/right
- Subalare - left/right
- Subnasale - left/right

If a pseudocode based on geometric properties exists in the literature for a landmark, we extracted the pseudocode for that landmark from the literature and placed it on the Github page [40]. We studied the existing algorithms in the literature and implemented either an original algorithm or one similar to the algorithms presented in the literature. We listed the names of the articles that included pseudocode for a facial landmark and the originality of our algorithms in Table 1.

The implementations were done in Python (version 3.1), and Trimesh Python library [41] was used to load 3D models that are in Wavefront (.obj) format. The algorithms assume that the face 3D models are placed in the correct pose and orientation on the x , y , and z coordinate systems, facing the z -axis.

The algorithms utilize the geometric properties of the head to find landmark locations, and most of the algorithms depend on finding the location of another landmark. Once the location of the other landmark(s) is found, some facial statistics (mean and standard deviation) of distances between landmark locations are utilized to determine the location of the landmark. The statistics are mostly retrieved from facebase.org's 3D facial norm database [42], [43]. For various algorithms, we could not find measurement statistics at facebase.org about the landmarks that will help us guide our algorithms. For those, we calculated statistics based on our proprietary 3D model dataset that includes 115 3D facial scans of adults. The list of the statistics used while locating the landmarks

and the dependent landmarks that need to be located before the landmark are listed in Table 2. Figure 2 depicts the hierarchy of dependencies between the landmarks. As shown in Figure 2 (and in Table 2), almost all algorithms utilize the location of Pronasale, and many algorithms depend on locating Subnasale.

III. PSEUDOCODE FOR LANDMARK DETECTION

In this section, we present the description of the landmarks and their pseudocode:

A. ALAR FLARE (ALARE) (LEFT/RIGHT)

Alar Flare (Alare) is the most lateral point on the left and right ala of the nose [20].

Pseudocode:

1. Locate the Pronasale and Subnasale.
2. Select all vertices that are above the Subnasale's y -coordinate, and between the Subnasale's z -coordinate and the Pronasale's z -coordinate.
3. Sort the vertices by x -coordinate.
4. Assign the leftmost vertex as the Alar Flare Left.
5. Assign the rightmost vertex as the Alar Flare Right.

B. ALAR BASE JUNCTION/ALAR CREASE (LEFT/RIGHT)

Alar base is the junction between the alar crease and the cheek [20].

Pseudocode:

1. Find the subnasale.
2. Select vertices slightly above and to the left of the subnasale based on the subnasal width statistics
3. Sort the vertices by x
4. Assign the vertex with a relative z minima as the left subalare
5. Select vertices slightly above and to the right of the subnasale based on the subnasal width statistics
6. Sort the vertices by x
7. Assign the vertex with a relative z minima as the right subalare

C. ALAR RIM'S HIGHEST POINT (LEFT/RIGHT)

The highest point of the left alar rim [20].

Pseudocode:

1. Find the subnasale
2. Select vertices diagonal-left above the subnasale using Nasal Width (Right Alare (al_r) to Left Alare (al_l)) statistical data from facebase.org
3. Sort the vertices multidimensionally using both x and y in quadrant 1, i.e. sort by $x + y$
4. Assign the uppermost x and y vertex as the left alar rim's highest point
5. Select vertices diagonal-right above the subnasale using Nasal Width (Right Alare (al_r) to Left Alare (al_l)) statistical data from facebase.org
6. Sort the vertices multidimensionally using both x and y in quadrant 4, i.e. sort by $x - y$

Assign the uppermost x and y vertex as the right alar rim's highest point.

D. CHEILION (LEFT/RIGHT)

Cheilion is the landmark located at the oral commissure where the upper and lower lips meet on left/right side of the gently closed lips [20].

Pseudocode:

1. Find the stomion.
2. Select vertices on the left of the stomion with similar x -values based on the Labial Fissure Width statistics.
3. Find a vertex with a relative z minimum or a z -value lower than the stomion.
4. Assign this vertex as the left cheilion.
5. Select vertices on the right of the stomion with similar x -values based on the Labial Fissure Width statistics.
6. Find a vertex with a relative z minimum or a z -value lower than the stomion.
7. Assign this vertex as the right cheilion.

E. COLUMELLAR RIM (LEFT/RIGHT)

They are the lowest points (or widest points) of the left and right nostrils, as seen from the lateral view on the columellar side at the mucocutaneous junction [20].

Pseudocode:

1. Find the pronasale.
2. Select vertices diagonally downwards to the left of the pronasale using statistical data from proprietary dataset.
3. Sort the vertices by both x and y coordinates, using quadrant 4 (i.e., sort by $x - y$).
4. Assign the last vertex as the left columellar rim.
5. Select vertices diagonally downwards to the right of the pronasale using statistical data from proprietary dataset.
6. Sort the vertices by both x and y coordinates, using quadrant 1 (i.e., sort by $x + y$).
7. Assign the first vertex as the right columellar rim.

F. COLUMELLAR BREAK POINT

Columellar break point is the point in the columellar region of the nose where the tip of the nose stops curving, and the columellar linear structure begins, in the midline [20].

Pseudocode:

1. Find the subnasale.
2. Select vertices above the subnasale using statistical data.
3. Sort the vertices by y .
4. Assign the largest y as the columellar break point.

G. ENDOCANTHION (LEFT/RIGHT)

Endocanthion is the inner corners of the eye where the upper and lower eyelids meet [20]. In the literature, it is also known as Medial Canthus.

Pseudocode:

1. Find the sellion
2. Starting from the sellion, select vertices to the left in a region defined based on the 'Inter-canthal Width' statistics from facebase.org's 3D norms database.
3. First, select a region that is away by the mean value of 'Inter-canthal Width' from the sellion. If a local minimum is not found, expand the region by standard deviation of 'Inter-canthal Width' at each iteration.
4. When the vertex that satisfies the local minima condition (x value is larger than next two vertices and smaller than previous two vertices) is found, assign this vertex as the left endocanthion.
5. Repeat the same process in the opposite direction to find the right endocanthion.

H. EXOCANTHION (LEFT/RIGHT)

Exocanthion is the outer corner of the eye where the upper and lower eyelids meet [20]. In the literature, it is also known as Lateral Canthus.

Pseudocode:

1. Find the sellion.
2. Starting from the sellion, select vertices to the left in a region defined based on the 'Outer-canthal Width' statistics from facebase.org's 3D norms database.
3. First, select a region that is a certain distance from the sellion, based on the mean value of 'Inter-canthal Width'. If a local minimum is not found, expand the region by the standard deviation of 'Outer-canthal Width' at each iteration.
4. When a vertex that satisfies the local minimum condition (its x value is larger than the next two vertices and smaller than the previous two vertices) is found, assign it as the left exocanthion.
5. Repeat the same process in the opposite direction to find the right exocanthion.

I. GLABELLA

Glabella is the most prominent point of the forehead in the midline between the eyebrows [20].

Pseudocode:

1. Find the pronasale.
2. Select vertices above the pronasale.
3. Assign the vertex with a relative maximum z-value as the glabella.

J. GNATHION (MENTON)

Gnathion (menton) is the lowest point on the soft tissue profile of the chin in mid-sagittal plane [20].

Pseudocode:

1. Find the pronasale
2. Select vertices based on the stats from facebase.org that gives the distance between the pronasale and gnathion: [lower face height + nasal height - nasal bridge length].
3. Find the lowest relative maxima for z.
4. Assign this vertex as the gnathion.

K. LABIALE SUPERIUS

Labiale superius is the midline point representing the mucocutaneous vermilion border of the upper lip [20].

Pseudocode:

1. Find the subnasale.
2. Select vertices below the subnasale based on the Philtrum Length statistics from the selection region, which will be determined by the mean value of Philtrum Length.
3. Find the vertex with a relative maximum for the z-coordinate.
4. If a vertex with a relative maximum for z cannot be found, expand the region by one standard deviation of Philtrum Length.
5. When a vertex with a relative maximum for z is found, assign it as the labiale superius.

L. LATERAL HELIX OF EAR (LEFT/RIGHT)

The helix of ear (left/right) is the utmost point on the helix of the left ear [20].

Pseudocode:

1. Use the minimum and maximum y-values of the vertices, along with the statistics of nasal bridge length, to find the region along the y-axis that will include the lateral helix of the ear.
2. Within this region, find the vertex with the largest x-value within one standard deviation from the midpoint.
3. Assign this vertex as the left lateral helix.
4. Within this region, find the vertex with the smallest x-value within one standard deviation from the midpoint.
5. Assign this vertex as the right lateral helix.

M. MAXILLOFRONTALE (LEFT/RIGHT)

Maxillofrontale is the point where the maxilloanterior and nasoanterior sutures meet [20].

Pseudocode:

1. Find the pronasale and endocanthion.
2. Select vertices at the y-coordinate level of the endocanthion and to the left of the pronasale using statistics from proprietary dataset.
3. Sort the vertices by x-coordinate.
4. Assign the last vertex as the left maxillofrontale.
5. Select vertices at the y-coordinate level of the endocanthion and to the right of the pronasale using statistics from proprietary dataset.
6. Sort the vertices by x-coordinate.
7. Assign the first vertex as the right maxillofrontale.

N. NASAL PARENTHESIS-LEFT/RIGHT

Nasal parenthesis is the summit of the left/right nasal parentheses/canthal-alar line.

Pseudocode:

1. Find the pronasale.
2. Select vertices diagonally upwards to the left of the pronasale using statistics from proprietary dataset.
3. Sort the vertices by both x and y coordinates, using quadrant 1 (i.e., sort by $x + y$).
4. Assign the last vertex as the left nasal parenthesis.
5. Select vertices diagonally upwards to the right of the pronasale using statistics from proprietary dataset.
6. Sort the vertices by both x and y coordinates, using quadrant 4 (i.e., sort by $x - y$).
7. Assign the first vertex as the right nasal parenthesis.

O. NASION (RADIX)

Nasion (Radix) is the midpoint of the nasofrontal suture line where the frontal bone and nasal bones join [20].

In some of the literature, Nasion (Radix) and Sellion are considered the same landmark. There are no geometric properties on the surface of the face that can be utilized to distinguish Nasion from Sellion. Therefore, we accepted Sellion and the Nasion as the same landmark. When the location of Nasion is needed, our implementation calls the function for Sellion and returns the location of the Sellion. Therefore, the pseudocode for Sellion is the same as Nasion. Nasion landmark is not counted for the total landmark count (thirty-eight) in this study.

P. PRONASALE (TIP)

Pronasale (tip) is the most protrusive point on the nasal tip in the midline [20].

Pseudocode:

1. Determine the minimum and maximum x and y coordinates (\min_x , \max_x , \min_y , \max_y) of the vertices.
2. Define a region where the nose is approximately centered by calculating the coordinates ($\text{center} = (\min_x + \max_x)/2$, $y = (\min_y + \max_y)/3$).
3. Sort the vertices within the defined region and locate the vertex with the highest z value. Assign this vertex as the Pronasale.

Q. SELLION

Sellion is the deepest depression of the nasal bones and often coincides with soft tissue nasion [20].

Pseudocode:

1. Locate the Pronasale.
2. Starting from the Pronasale, use the nasal bridge length statistics (Nasion (n) to Pronasale (prn)) from facebase.org to establish a search region with one standard deviation of nasal bridge length.
3. Iterate through the search region on the increasing y-axis until a relative minimum for the z-coordinate is found.
4. If a relative minimum is not found in the initial search region, expand the search region by one standard deviation of nasal bridge length.
5. If a relative minimum is found, assign the vertex in the search region as the Sellion.

R. SUBNASALE

Subnasale is the deepest point at the junction of the base of the columella and the upper lip in the midline [20].

Pseudocode:

1. Locate the Pronasale.
2. Define the height and depth of the search region based on the Nasal height (Nasion (n) to Subnasale (sn)) and Nasal bridge length (Nasion (n) to Pronasale (prn)) statistics, as well as the Nasal Protrusion (Pronasale (prn) to Subnasale (sn)) statistics from facebase.org.
3. Search for an inflection point on the z-axis below the y-axis of the Pronasale, in decreasing order. (Note that this algorithm might only work if the y-axis of the Pronasale is less than the y-axis of the Subnasale. Some nose shapes, such as those with a drooping tip, may have this property).
4. Assign this vertex as the Subnasale.

S. STOMION

The point at which the upper and lower lip make contact in the midline on gently closed lips [20].

Pseudocode:

1. Find the labiale superius
2. Select vertices below the labiale superius based on the Upper Vermilion Height (Labiale Superius (ls) - Stomion (sto)) statistics from facebase.org
3. Find the first vertex with a relative z minima
4. Assign this vertex as the stomion

T. SUBALARE (LEFT/RIGHT)

Subalare is the point at the lower limit of each alar base, where the alar base disappears into skin of the upper lip. It is a bilateral landmark located below the nostril opening at the point where the infero-medial continuation of the alar cartilage inserts into the skin of the upper lip [20].

Pseudocode:

1. Find the subnasale.
2. Select vertices slightly above and to the left of the subnasale based on the subnasal width statistics.
3. Sort the vertices by x .
4. Assign the vertex with a relative z minima as the left subalare.
5. Select vertices slightly above and to the right of the subnasale based on the subnasal width statistics.
6. Sort the vertices by x .
7. Assign the vertex with a relative z minima as the right subalare.

U. SUBNASALE (LEFT/RIGHT)

Subnasale left/right are the points where the right/left columella meets the nostril sill [20].

Pseudocode:

1. Locate the Subnasale.
2. Select vertices to the left based on the 'subnasale width' (Right Subalare (sbal_r) to Left Subalare (sbal_l)) statistics from facebase.org's 3D norms database. Since the Subnasale is approximately half the distance to the Subalare from the Subnasale, divide the 'subnasale width' by 2.
3. Sort the vertices by increasing x-coordinate.
4. Assign the vertex with the largest x-coordinate as the Subnasale left.
5. Select vertices to the right based on the 'subnasale width' statistics from facebase.org's 3D norms database.
6. Sort the vertices by decreasing x-coordinate.
7. Assign the vertex with the smallest x-coordinate as the Subnasale right.

V. SUPRATIP BREAK POINT

Supratip break point is the area just cephalad to the nasal tip at the caudal portion of the nasal dorsum.

Pseudocode:

1. Find the pronasale.
2. Select vertices above the pronasale using statistics from proprietary dataset.
3. Sort the vertices by y-coordinate.
4. Assign the last vertex as the supratip break point.

W. TIP DEFINING POINT (LEFT/RIGHT)

The nasal tip defining point is the most anterior projection of the tip cartilages, usually corresponding to the apex of the lobular arch anatomically, and is typically identified externally where the light reflex is seen on the nasal tip.

Pseudocode:

1. Find the pronasale
2. Select vertices above and to the left of the pronasale using statistics from proprietary dataset.
3. Sort the vertices by y-coordinate
4. Assign the last vertex as the left tip defining point.
5. Select vertices above and to the right of the pronasale using statistics from proprietary dataset.

6. Sort the vertices by y-coordinate
7. Assign the last vertex as the left tip defining point.

X. TRICHION

The trichion is the point on the hairline in the midline of the forehead.

Pseudocode:

1. Find the glabella
2. Select vertices above the glabella between the glabella and trichion based on the statistics
3. Search upwards to find the first vertex that has a significant z increase which indicates the existence of hair.

Y. ZYGION (LEFT/RIGHT)

Zygion is the most lateral point of the right zygomatic arch [20].

Pseudocode:

1. Find the pronasale.
2. Using the maximum facial width statistics (from right Zygion to left Zygion) from facebase.org, determine the x-coordinate value of the left zygion.
3. Using statistics, determine the y-coordinate value of the left zygion.
4. Select all vertices in the region based on the x and y coordinate values.
5. Sort the vertices by both x and y coordinates, using quadrant 1 (i.e., sort by x + y).
6. Assign the vertex as the left zygion.
7. Using the maximum facial width statistics (from right Zygion to left Zygion) from facebase.org, determine the x-coordinate value of the right zygion.
8. Using statistics, determine the y-coordinate value of the right zygion.
9. Select all vertices in the region based on the x and y coordinate values within a diagonal line to the approximate location.
10. Sort the vertices by both x and y coordinates, using quadrant 4 (i.e., sort by x - y).
11. Assign the vertex as the right zygion.

IV. RESULTS AND DISCUSSION

We have tested the algorithms on 111 facial 3D models for the thirty-eight landmarks. The temporal analysis of algorithms shows that it takes on average 0.5 seconds to locate a landmark at the first level (e.g. Pronasale), 0.8 seconds to locate a landmark at the second level (e.g. Subnasale), and 1.1 seconds for a landmark at the third level shown in Figure 2 when the algorithm is executed on a Jupyter Notebook page using the Python 3.1 kernel at MacBook Pro with M1 Max Chip and 32GB memory.

We calculate the error by finding the distance between the manual markings and the location found by the algorithm. The mean error for each landmark is calculated using the formula below. In this formula, x_{mi} , y_{mi} , and z_{mi} represent the coordinates of manual markings and x_{ai} , y_{ai} , and z_{ai} represent

TABLE 3. Statistical conclusions for facial landmarks errors.

Facial Landmark	mean	median	std	min	max
Pronasale/Tip	1.98	1.82	1.13	0	5.25
Tip Defining Point-					
left	3.45	2.84	2.12	0.08	10.64
Supratip Break Point	3.75	3.06	2.44	0.15	11.96
Columellar Break					
Point	3.87	3.38	2.47	0.18	13.06
Labiale Superius	4.28	3.92	2.21	0.2	10.32
Nasal Parenthesis –					
left	5.16	4.67	2.81	0.1	14.94
Glabella	5.54	4.98	3.93	0.41	24.88
Subnasale	5.58	5.64	2.1	0.32	11.14
Stomion	5.59	5.41	2.52	1.01	12.99
Endocanthion – left	5.94	5.24	3.23	0.35	14.12
Alare/Alar Flare – left	6.99	6.29	3.94	0.89	21.12
Subnasale – left	7.13	6.53	2.97	1.17	15.55
Alar Rim’s Highest					
Point – left	7.2	6.49	3.74	0.69	18.47
Subalare – left	7.25	7.23	3.51	0.77	15.11
Cheilion – left	8.06	7.81	3.92	0.85	22.27
Zygion – left	8.08	7.35	4.48	0.32	23.43
Exocanthion – left	9.24	8.11	5.1	0.38	24.01
Maxillofrontale – left	10.04	9.58	4.09	1.7	19
Trichion	10.19	7.72	9.12	1.28	52.71
Columellar Rim - left	10.31	10.33	3.1	3.4	19.42
Alar Base Junction -					
left	11.11	10.9	3.01	3.2	19.49
Sellion	11.4	11.14	4.21	3.23	21.59
Gnathion	11.56	9.41	8.43	0.22	41.21
Lateral helix of ear -					
left	18.16	12.87	15.8	0	85.63

the coordinates found by the algorithm.

$$\frac{1}{n} \sum_{i=1}^n \sqrt{(x_{mi} - x_{ai})^2 + (y_{mi} - y_{ai})^2 + (z_{mi} - z_{ai})^2}$$

Table 3 presents the mean, median, standard deviation, minimum, and maximum values of the errors for the 111 samples. The values are in millimeters and the table is sorted based on the mean values. The algorithms for bilateral landmarks work with the same logic for the left and right landmarks, and hence their results are very similar. Therefore, we only present the results for the left of the bilateral landmarks.

The mean is almost always larger than the median due to the outliers in the errors. The maximum values in Table 3 indicate the extent of the outliers. We had the most outliers for the lateral helix of the ear and trichion landmarks. As we investigated the cause, we noticed that the heuristic of the algorithm lateral helix of the ear did not work since the minimum and maximum points on the x-axis were not always the ear on the 3D scan due to hair. We also noticed that the heuristic of the trichion also did not work due to lack of hair or due to hair not being tied back during the 3D scan as the algorithm detects the changes in the z-axis caused by the hair.

Figure 3 provides the histogram of error values to show the distribution of the error values and outliers. According to Figure 3, the largest errors and outliers exist for the lateral helix of the ear, trichion, and gnathion landmarks. The smallest errors exist for the Pronasale, which is a good sign since almost all landmarks depend on detecting the Pronasale

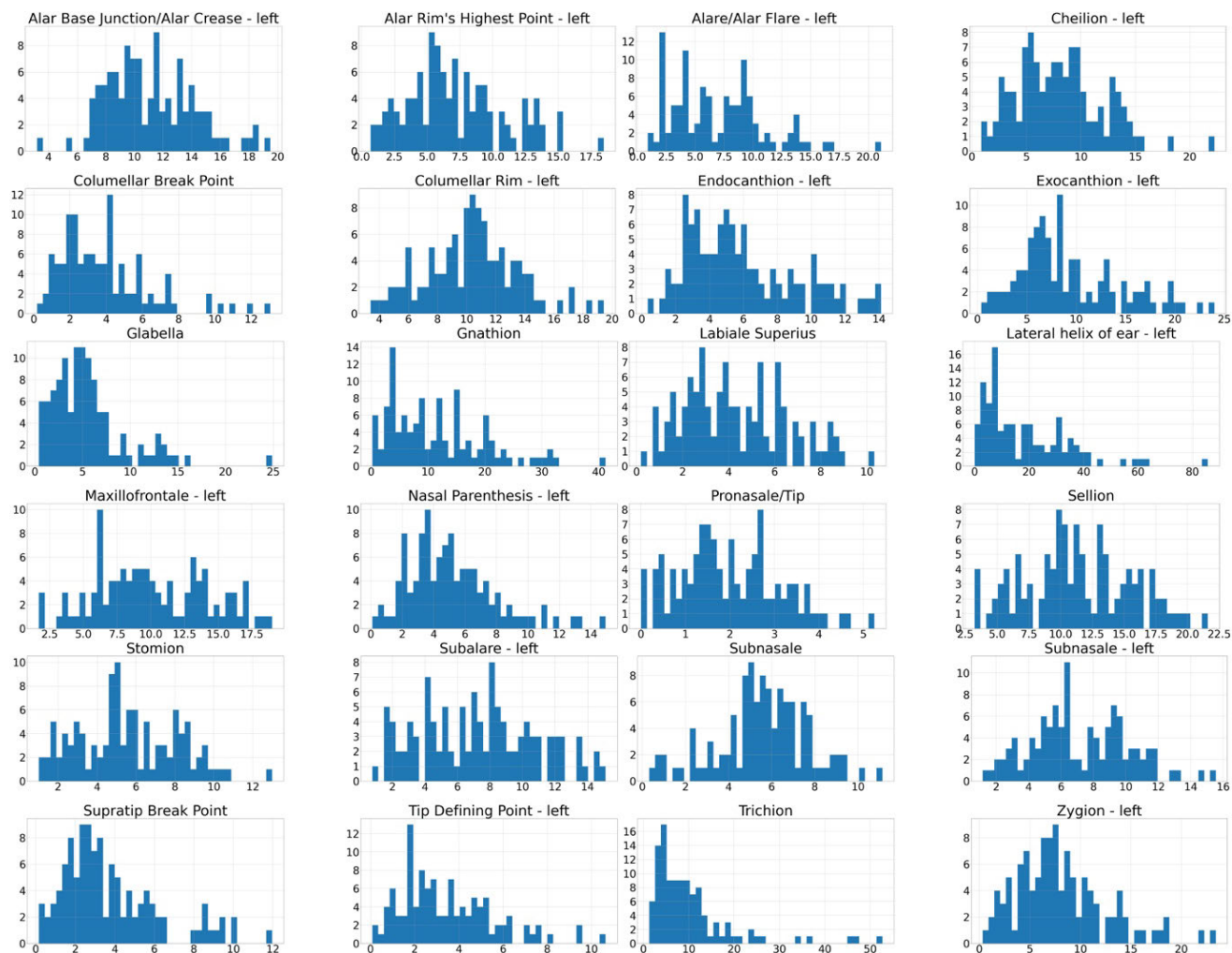


FIGURE 3. The histogram of errors (distance between the manual markings and results of the algorithms) The bilateral landmarks are shown only once. From top left to bottom right: Alar Base Junction/Alar Crease, Alar Rim's Highest Point, Alare/Alar Flare, Cheilion, Columellar Break Point, Columellar Rim, Endocanthion, Exocanthion, Glabella, Gnathion/Menton, Labiale Superius, Lateralhelix of ear, Maxillofrontale, Nasal Parenthesis, Pronasale, Sellion, Stomion, Subalare, Subnasale, Subnasale, Supratip Break Point, Tip Defining Point, Trichion, Zygion.

first. The Subnasale, which is another landmark that many landmarks depend on, does not have high error.

While we compare our results with manual markings, note that manual markings can have errors. The markings can also slightly change from one rater (the person who does the marking) to another, and the reliability of the raters should be tested [44]. To achieve more accurate manual markings, several raters could be utilized, and then the average of the markings could be computed to reach a consensus.

To reduce the results, the utilization of statistics can be extended to incorporate more heuristics. For example, statistics about the average face width and height were utilized to estimate the difference between the x and y coordinates of the Zygion and the Pronasale landmarks.

We could improve this by first determining how wide and long the subject's face is when compared to the average face width and height, and then better estimate the x and y coordinates of the Zygion given the x and y coordinates of the Pronasale utilizing the ratio of the subject's face and

the average face values. Similar statistics and heuristics can be utilized for other landmarks based on the ratio of the subject's measurement and the average of that measurement to compute the location of the landmark.

The performance of the algorithms can further be improved if the age, gender, and ethnicity of the subject are known or can be estimated by utilizing statistics for the subject's age, gender and ethnicity.

V. CONCLUSION

In this study, we developed algorithms to detect facial landmarks based on geometric properties and facial statistics. Facial landmark detection is widely applied in fields, such as face recognition, face surgery, biometrics, and surveillance systems. We reviewed the pseudocode of algorithms in the current literature. and developed algorithms for thirty-eight landmarks using geometric properties and statistical information about facial measurements. The algorithms for thirty landmarks are original contributions to the literature.

To facilitate replication and further research, we have made the python source codes available to other researchers on GitHub [40]. The accuracy of our algorithms was evaluated through the analysis of 111 3D face scans.

To the best of our knowledge, this study covers the largest number of facial landmark detection algorithms based on the geometric properties of 3D models. This is the first study that provides the implementation of the algorithms along with detailed pseudocode.

The results indicate that the geometric properties of the face and the facial statistics can be utilized to discover many landmark locations, and the output of high-performing algorithms, such as Pronasale, can be combined with outputs of other approaches, such as machine learning approaches to provide a more robust solution for facial landmark detection.

ACKNOWLEDGMENT

The authors would like to thank Philip Sawyer, Joshua Palmer, and Aidan Beeching for their help in reviewing the existing literature for the pseudocode of the facial landmark algorithms.

REFERENCES

- [1] M. Lal, K. Kumar, R. Hussain, A. Maitlo, S. Ali, and H. Shaikh, "Study of face recognition techniques: A survey," *Int. J. Adv. Comput. Sci. Appl.*, vol. 9, no. 6, 2018, doi: [10.14569/ijacsa.2018.090606](https://doi.org/10.14569/ijacsa.2018.090606).
- [2] G. Lekakis, G. Hens, P. Claes, and P. W. Hellings, "Three-dimensional morphing and its added value in the rhinoplasty consult," *Plastic Reconstructive Surg.-Global Open*, vol. 7, no. 1, p. e2063, Jan. 2019, doi: [10.1097/gox.0000000000002063](https://doi.org/10.1097/gox.0000000000002063).
- [3] Y. Jing, X. Lu, and S. Gao, "3D face recognition: A survey," 2021, *arXiv:2108.11082*.
- [4] S. Zhou and S. Xiao, "3D face recognition: A survey," *Hum.-Centric Comput. Inf. Sci.*, vol. 8, no. 1, Nov. 2018, doi: [10.1186/s13673-018-0157-2](https://doi.org/10.1186/s13673-018-0157-2).
- [5] E. R. Manal, Z. Arsalane, and M. Aicha, "Automated detection of craniofacial landmarks on a 3D facial mesh," in *Proc. Int. Conf. Integr. Design Prod. (Lecture Notes in Mechanical Engineering)*. Nov. 2020, pp. 537–548, doi: [10.1007/978-3-030-62199-5_47](https://doi.org/10.1007/978-3-030-62199-5_47).
- [6] E. Vezzetti, F. Marcolin, S. Tornincasa, L. Ulrich, and N. Dagnes, "3D geometry-based automatic landmark localization in presence of facial occlusions," *Multimedia Tools Appl.*, vol. 77, no. 11, pp. 14177–14205, Jul. 2017, doi: [10.1007/s11042-017-5025-y](https://doi.org/10.1007/s11042-017-5025-y).
- [7] E. R. Manal, Z. Arsalane, and M. Aicha, "Survey on the approaches based geometric information for 3D face landmarks detection," *IET Image Process.*, vol. 13, no. 8, pp. 1225–1231, May 2019, doi: [10.1049/iet-ipr.2018.6117](https://doi.org/10.1049/iet-ipr.2018.6117).
- [8] P. Perakis, G. Passalis, T. Theoharis, and I. Kakadiaris, "3D facial landmark detection & face registration a 3D facial landmark model & 3D local shape descriptors approach," *Comput. Graph. Lab., Univ. Athens, Athens, Greece, Tech. Rep. TP-2010-01*, 2010.
- [9] T. Terada, Y.-W. Chen, and R. Kimura, "3D facial landmark detection using deep convolutional neural networks," in *Proc. 14th Int. Conf. Natural Comput., Fuzzy Syst. Knowl. Discovery (ICNC-FSKD)*, Jul. 2018, doi: [10.1109/fskd.2018.8687254](https://doi.org/10.1109/fskd.2018.8687254).
- [10] R. R. Paulsen, K. A. Juhl, T. M. Haspang, T. Hansen, M. Ganz, and G. Einarsson, "Multi-view consensus CNN for 3D facial landmark placement," in *Computer Vision-(ACCV)*. 2018, pp. 706–719, 2019, doi: [10.1007/978-3-030-20887-5_44](https://doi.org/10.1007/978-3-030-20887-5_44).
- [11] H. Dai, N. Pears, K. A. Juhl, and W. A. P. Smith, "3D morphable models: The face, ear and head," in *3D Imaging, Analysis and Applications*. vol. 2020, pp. 463–512, doi: [10.1007/978-3-030-44070-1_10](https://doi.org/10.1007/978-3-030-44070-1_10).
- [12] G. Hu, "Face analysis using 3D morphable models," Ph.D. thesis, *Fac. Eng. Phys. Sci., Univ. Surrey, Guildford, U.K.*, Apr. 2015, pp. 1–112. [Online]. Available: <http://www.ee.surrey.ac.uk/CVSSP/Publications/papers/Hu-thesis-2015.pdf>
- [13] J. Booth, A. Roussos, S. Zafeiriou, A. Ponniah, and D. Dunaway, "A 3D morphable model learnt from 10,000 faces," in *Proc. IEEE Conf. Comput. Vis. Pattern Recognit. (CVPR)*, Jun. 2016, pp. 5543–5552, doi: [10.1109/CVPR.2016.598](https://doi.org/10.1109/CVPR.2016.598).
- [14] J. Booth, A. Roussos, A. Ponniah, D. Dunaway, and S. Zafeiriou, "Large scale 3D morphable models," *Int. J. Comput. Vis.*, vol. 126, nos. 2–4, pp. 233–254, Apr. 2017, doi: [10.1007/s11263-017-1009-7](https://doi.org/10.1007/s11263-017-1009-7).
- [15] A. Géron, *Hands-on Machine Learning With Scikit-Learn and TensorFlow: Concepts, Tools, and Techniques to Build Intelligent Systems*. Sebastopol, CA, USA: O'Reilly Media, 2019.
- [16] A. Abu, C. G. Ngo, N. I. A. Abu-Hassan, and S. A. Othman, "Automated craniofacial landmarks detection on 3D image using geometry characteristics information," *BMC Bioinf.*, vol. 19, no. S13, pp. 65–80, Feb. 2019, doi: [10.1186/s12859-018-2548-9](https://doi.org/10.1186/s12859-018-2548-9).
- [17] S. Gupta, M. K. Markey, and A. C. Bovik, "Anthropometric 3D face recognition," *Int. J. Comput. Vis.*, vol. 90, no. 3, pp. 331–349, 2010, doi: [10.1007/s11263-010-0360-8](https://doi.org/10.1007/s11263-010-0360-8).
- [18] S. Liang, J. Wu, S. M. Weinberg, and L. G. Shapiro, "Improved detection of landmarks on 3D human face data," in *Proc. 35th Annu. Int. Conf. IEEE Eng. Med. Biol. Soc. (EMBC)*, Jul. 2013, pp. 6482–6485, doi: [10.1109/EMBC.2013.6611039](https://doi.org/10.1109/EMBC.2013.6611039).
- [19] M. Li, J. B. Cole, M. Manyama, J. R. Larson, D. K. Liberton, S. L. Riccardi, T. M. Ferrara, S. A. Santorico, J. J. Bannister, N. D. Forkert, R. A. Spritz, W. Mio, and B. Hallgrímsson, "Rapid automated landmarking for morphometric analysis of three-dimensional facial scans," *J. Anatomy*, vol. 230, no. 4, pp. 607–618, Apr. 2017, doi: [10.1111/joa.12576](https://doi.org/10.1111/joa.12576).
- [20] M. M. Celikoyar, M. F. Pérez, M. I. Akbaş, and O. Topsakal, "Facial surface anthropometric features and measurements with an emphasis on rhinoplasty," *Aesthetic Surg. J.*, vol. 42, no. 2, pp. 133–148, Apr. 2021, doi: [10.1093/asj/sjab190](https://doi.org/10.1093/asj/sjab190).
- [21] O. Topsakal, M. I. Akbaş, D. Demirel, R. Nunez, B. S. Smith, M. F. Perez, and M. M. Celikoyar, "Digitizing rhinoplasty: A web application with three-dimensional preoperative evaluation to assist rhinoplasty surgeons with surgical planning," *Int. J. Comput. Assist. Radiol. Surg.*, vol. 15, no. 11, pp. 1941–1950, Sep. 2020, doi: [10.1007/s11548-020-02251-7](https://doi.org/10.1007/s11548-020-02251-7).
- [22] S. Mehryar, K. Martin, and K. N. Plataniotis, "Automatic landmark detection for 3D face image processing," in *Proc. IEEE Congr. Evol. Comput.*, Jul. 2010, pp. 1–7, doi: [10.1109/CEC.2010.5586520](https://doi.org/10.1109/CEC.2010.5586520).
- [23] C. Creusot, N. Pears, and J. Austin, "3D face landmark labelling," in *Proc. ACM Workshop 3D Object Retr.*, Oct. 2010, pp. 27–32, doi: [10.1145/1877808.1877815](https://doi.org/10.1145/1877808.1877815).
- [24] M. P. Segundo, L. Silva, O. R. P. Bellon, and C. C. Queirolo, "Automatic face segmentation and facial landmark detection in range images," *IEEE Trans. Syst., Man, Cybern., B (Cybern.)*, vol. 40, no. 5, pp. 1319–1330, Oct. 2010, doi: [10.1109/TSMCB.2009.2038233](https://doi.org/10.1109/TSMCB.2009.2038233).
- [25] S. Berretti, B. Ben Amor, M. Daoudi, and A. del Bimbo, "3D facial expression recognition using SIFT descriptors of automatically detected keypoints," *Vis. Comput.*, vol. 27, no. 11, pp. 1021–1036, Jun. 2011, doi: [10.1007/s00371-011-0611-x](https://doi.org/10.1007/s00371-011-0611-x).
- [26] P. Perakis, G. Passalis, T. Theoharis, and I. A. Kakadiaris, "3D facial landmark detection under large yaw and expression variations," *IEEE Trans. Pattern Anal. Mach. Intell.*, vol. 35, no. 7, pp. 1552–1564, Jul. 2013, doi: [10.1109/TPAMI.2012.247](https://doi.org/10.1109/TPAMI.2012.247).
- [27] P. Perakis, T. Theoharis, and I. A. Kakadiaris, "Feature fusion for facial landmark detection," *Pattern Recognit.*, vol. 47, no. 9, pp. 2783–2793, Sep. 2014, doi: [10.1016/j.patcog.2014.03.007](https://doi.org/10.1016/j.patcog.2014.03.007).
- [28] C. Creusot, N. Pears, and J. Austin, "A machine-learning approach to keypoint detection and landmarking on 3D meshes," *Int. J. Comput. Vis.*, vol. 102, nos. 1–3, pp. 146–179, Mar. 2013, doi: [10.1007/s11263-012-0605-9](https://doi.org/10.1007/s11263-012-0605-9).
- [29] J. Guo, X. Mei, and K. Tang, "Automatic landmark annotation and dense correspondence registration for 3D human facial images," *BMC Bioinf.*, vol. 14, no. 1, p. 232, Dec. 2013, doi: [10.1186/1471-2105-14-232](https://doi.org/10.1186/1471-2105-14-232).
- [30] E. Sanginetto, "Pose and expression independent facial landmark localization using dense-SURF and the Hausdorff distance," *IEEE Trans. Pattern Anal. Mach. Intell.*, vol. 35, no. 3, pp. 624–638, Mar. 2013, doi: [10.1109/TPAMI.2012.87](https://doi.org/10.1109/TPAMI.2012.87).
- [31] E. Vezzetti and F. Marcolin, "Geometry-based 3D face morphology analysis: Soft-tissue landmark formalization," *Multimedia Tools Appl.*, vol. 68, no. 3, pp. 895–929, May 2012, doi: [10.1007/s11042-012-1091-3](https://doi.org/10.1007/s11042-012-1091-3).
- [32] E. Vezzetti and F. Marcolin, "3D landmarking in multiexpression face analysis: A preliminary study on eyebrows and mouth," *Aesthetic Plastic Surg.*, vol. 38, no. 4, pp. 796–811, May 2014, doi: [10.1007/s00266-014-0334-2](https://doi.org/10.1007/s00266-014-0334-2).

- [33] S. Moos, F. Marcolin, S. Tornincasa, E. Vezzetti, M. G. Violante, G. Fracastoro, D. Speranza, and F. Padula, "Cleft lip pathology diagnosis and foetal landmark extraction via 3D geometrical analysis," *Int. J. Interact. Des. Manuf. (IJIDeM)*, vol. 11, no. 1, pp. 1–18, Nov. 2014, doi: [10.1007/s12008-014-0244-1](https://doi.org/10.1007/s12008-014-0244-1).
- [34] S. Cheng, S. Zafeiriou, A. Asthana, and M. Pantic, "3D facial geometric features for constrained local model," in *Proc. IEEE Int. Conf. Image Process. (ICIP)*, Paris, France, Oct. 2014, pp. 1425–1429, doi: [10.1109/ICIP.2014.7025285](https://doi.org/10.1109/ICIP.2014.7025285).
- [35] S. Z. Gilani, F. Shafait, and A. Mian, "Shape-based automatic detection of a large number of 3D facial landmarks," in *Proc. IEEE Conf. Comput. Vis. Pattern Recognit. (CVPR)*, Boston, MA, USA, Jun. 2015, pp. 4639–4648, doi: [10.1109/CVPR.2015.7299095](https://doi.org/10.1109/CVPR.2015.7299095).
- [36] M. Galvánek, K. Furmanová, I. Chalás, and J. Sochor, "Automated facial landmark detection, comparison and visualization," in *Proc. 31st Spring Conf. Comput. Graph.*, Apr. 2015, pp. 7–14, doi: [10.1145/2788539.2788540](https://doi.org/10.1145/2788539.2788540).
- [37] F. M. Sukno, J. L. Waddington, and P. F. Whelan, "3-D facial landmark localization with asymmetry patterns and shape regression from incomplete local features," *IEEE Trans. Cybern.*, vol. 45, no. 9, pp. 1717–1730, Sep. 2015, doi: [10.1109/TCYB.2014.2359056](https://doi.org/10.1109/TCYB.2014.2359056).
- [38] X. Fan, Q. Jia, K. Huyen, X. Gu, and Z. Luo, "3D facial landmark localization using texture regression via conformal mapping," *Pattern Recognit. Lett.*, vol. 83, pp. 395–402, Nov. 2016, doi: [10.1016/j.patrec.2016.07.005](https://doi.org/10.1016/j.patrec.2016.07.005).
- [39] F. Marcolin and E. Vezzetti, "Novel descriptors for geometrical 3D face analysis," *Multimedia Tools Appl.*, vol. 76, no. 12, pp. 13805–13834, Jul. 2016, doi: [10.1007/s11042-016-3741-3](https://doi.org/10.1007/s11042-016-3741-3).
- [40] *3D Facial Landmark Detection Open Source Code on GitHub*. Accessed: Jan. 29, 2023. [Online]. Available: <https://github.com/research-digitized-rhinoplasty/3D-Facial-Landmark-Detection>
- [41] *Trimesh Phytion Library*. Accessed: Jan. 29, 2023. [Online]. Available: <https://github.com/mikedh/trimesh>
- [42] S. M. Weinberg, Z. D. Raffensperger, M. J. Kesterke, C. L. Heike, M. L. Cunningham, J. T. Hecht, C. H. Kau, J. C. Murray, G. L. Wehby, L. M. Moreno, and M. L. Marazita, "The 3D facial norms database: Part 1. A web-based craniofacial anthropometric and image repository for the clinical and research community," *Cleft Palate-Craniofacial J.*, vol. 53, no. 6, pp. 185–197, Nov. 2016, doi: [10.1597/15-199](https://doi.org/10.1597/15-199).
- [43] B. D. Samuels, R. Aho, J. F. Brinkley, and A. Bugacov, "FaceBase 3: Analytical tools and FAIR resources for craniofacial and dental research," *Development*, vol. 147, no. 18, Sep. 2020, Art. no. dev191213, doi: [10.1242/dev.191213](https://doi.org/10.1242/dev.191213).
- [44] O. Topsakal, M. İ. Akbaş, B. S. Smith, M. F. Perez, E. C. Guden, and M. M. Celikoyar, "Evaluating the agreement and reliability of a web-based facial analysis tool for rhinoplasty," *Int. J. Comput. Assist. Radiol. Surg.*, vol. 16, no. 8, pp. 1381–1391, Jun. 2021, doi: [10.1007/s11548-021-02423-z](https://doi.org/10.1007/s11548-021-02423-z).



OGUZHAN TOPSAKAL (Member, IEEE) received the B.S. degree in computer engineering from Istanbul Technical University, Turkey, in 1996, and the M.S. and Ph.D. degrees in computer science from the University of Florida, in 2003 and 2007, respectively.

After gaining extensive experience in the software industry, he is currently an Assistant Professor with the Department of Computer Science, Florida Polytechnic University. He teaches courses

related to machine learning, algorithm design, database, and mobile development. His research interests include the applications of machine learning and deep learning.



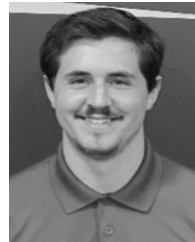
TAHIR CETIN AKINCI (Senior Member, IEEE) received the B.S. degree in electrical engineering from Klaipeda University, Lithuania, and the M.S. and Ph.D. degrees, in 2005 and 2010, respectively.

He was a Research Assistant with Marmara University, Istanbul, Turkey, from 2003 to 2010, and an Associate Professor with Istanbul Technical University (ITU), from 2016 to 2021. He has been a Full Professor with the Department of Electrical Engineering, ITU, since 2021. He has been a

Visiting Scholar with the University of California at Riverside (UCR), since 2021. His research interests include artificial neural networks, deep learning, machine learning, image processing, cognitive systems, signal processing, and data analysis.



JOSHUA MURPHY is currently pursuing the B.S. degree in computer science with a minor in software engineering with Florida Polytechnic University, Lakeland, FL, USA. While at Florida Polytechnic University, he worked as a Research Assistant to Dr. Oguzhan Topsakal, where he created various algorithms to detect landmarks on the face. He also worked on implementing various features for a website to analyze and evaluate the effectiveness of facial surgeries.



TAYLOR LEE-JAMES PRESTON is currently pursuing the B.S. degree with the Department of Computer Science, Florida Polytechnic University, Lakeland, FL, USA. He was a Research Assistant to Dr. Oguzhan Topsakal, in 2022, during which he helped Dr. Oguzhan Topsakal develop and test algorithms to locate specific landmarks on facial 3-D models.



MEHMET MAZHAR CELIKOYAR received the degree from the Hacettepe School of Medicine, Ankara, Turkey, in 1982. Then, he specialized in otolaryngology-head and neck surgery with Sislci Children's Hospital and Marmara University Hospital, in 1989. He had his fellowship training in head and neck surgery and facial plastic and reconstructive surgery with Methodist Hospital, Indianapolis, IN, USA, in 1996. Since 1996, he has been practicing in Istanbul. He is currently an

Otolaryngologist-Head and Neck Surgeon practicing with Istanbul Florence Nightingale Hospital. He is also one of the teaching members of the Department of Otolaryngology-Head and Neck Surgery, School of Medicine, Demiroglu Bilim University, Istanbul, Turkey. His recent activities include studies involved in integrating rhinoplasty with computer science.

...